

Black prismatic crystals of  $[\text{Ni}(\text{R},\text{R}\text{-chxn})_2\text{Br}]_n$  (**1**) were grown by slow diffusion of  $\text{Br}_2$  gas into 2-methoxyethanol solution of  $[\text{NiBr}_2(\text{R},\text{R}\text{-chxn})_2]$  under  $\text{N}_2$  atmosphere. Orange red crystals of  $[\text{NiBr}_2(\text{[14]aneN}_4)]\text{ClO}_4$ , **2**,<sup>9</sup> which is the reference compound containing a discrete  $\text{Ni}^{\text{III}}$  complex, were obtained by oxidizing  $[\text{Ni}(\text{[14]aneN}_4)](\text{ClO}_4)_2$  with  $\text{Br}_2$  in aqueous solution.

Single-crystal X-ray structure analyses were carried out at room temperature and  $-152^\circ\text{C}$  for **1**<sup>10</sup> and at room temperature for **2**.<sup>11</sup> The structure of **1** was refined by using a full-matrix least-squares technique including occupancy factors of the counter and bridging Br atoms. The stoichiometric structure of **1** was determined by the analysis and confirmed by both the elemental analysis<sup>12</sup> and the observed density.<sup>13</sup>

The chain structure of **1**, which is isomorphous with the mixed-valence compound of  $[\text{Pt}(\text{R},\text{R}\text{-chxn})_2][\text{PtCl}_2(\text{R},\text{R}\text{-chxn})_2]\text{Cl}_4$ <sup>14</sup> except for the position of a bridging halogen atom, is shown in Figure 1. The  $\text{Ni}(\text{R},\text{R}\text{-chxn})_2$  moieties, lying on special positions, are bridged by Br atoms and stacked along the *b*-axis, constructing a linear chain structure. The neighboring  $\text{Ni}(\text{R},\text{R}\text{-chxn})_2$  moieties on the same chain are linked by four  $\text{NH}\cdots\text{Br}\cdots\text{HN}$  hydrogen bonds (3.415 (12), 3.502 (12) Å). As shown in Figure 1, the hydrogen bond network extended over the chains constructs a two-dimensional structure parallel to the *bc* plane.

In order to discuss the physical properties of **1**, it is essential to decide whether the bridging Br atom is located at the midpoint between two Ni atoms or just deviated from the midpoint.<sup>15</sup> If the bridging Br atom is shifted slightly from the midpoint, the compound can be regarded as the well-known Peierls distorted halogen-bridged  $\text{Ni}^{\text{II}}\text{-X}\text{-Ni}^{\text{IV}}$  mixed-valence compound. On the other hand, the location of the atom at the midpoint would result in a halogen-bridged  $\text{Ni}^{\text{III}}\text{-X}\text{-Ni}^{\text{III}}$  compound with different properties. On the basis of careful consideration of the X-ray diffraction results,<sup>16</sup> we found that **1** has the  $\text{Ni}^{\text{III}}\text{-X}\text{-Ni}^{\text{III}}$  structure. Firstly, the  $\text{Ni}^{\text{III}}\text{-Br}$  distance of the chain compound **1** (2.580 (1) Å) is significantly shorter than that of the discrete

(8) A related Ni compound, which has the same crystal structure but is different in stoichiometry, has been reported: Toftlund, H.; Simonsen, O. *Inorg. Chem.* **1984**, *23*, 4261-4265.

(9) [14]aneN<sub>4</sub> denotes a macrocyclic ligand of 1,4,8,11-tetraazacyclotetradecane.

(10) X-ray structure analyses have been carried out by using a black prism with dimensions of  $0.19 \times 0.18 \times 0.10$  mm at room temperature and  $-152^\circ\text{C}$ . Crystal data are as follows: (1)  $\text{C}_{12}\text{H}_{28}\text{N}_4\text{NiBr}_3$ , orthorhombic, *I*222, *Z* = 2; at  $25^\circ\text{C}$ , *a* = 23.587 (5) Å, *b* = 5.161 (2) Å, *c* = 7.121 (1) Å, *V* = 866.8 (4) Å<sup>3</sup>, *D<sub>x</sub>* = 2.018 g cm<sup>-3</sup>, *D<sub>m</sub>* = 1.988 g cm<sup>-3</sup>,  $\mu(\text{Mo K}\alpha)$  = 84.50 cm<sup>-1</sup>; at  $-152^\circ\text{C}$ , *a* = 23.501 (4) Å, *b* = 5.157 (1) Å, *c* = 7.090 (1) Å, *V* = 859.3 (3) Å<sup>3</sup>, *D<sub>x</sub>* = 2.036 g cm<sup>-3</sup>,  $\mu(\text{Mo K}\alpha)$  = 85.24 cm<sup>-1</sup>. Intensity data were collected on a Rigaku AFC-5 four-circle diffractometer with graphite monochromated Mo K $\alpha$  radiation, equipped with a variable temperature apparatus based on a cold nitrogen gas stream method. The structure was solved by a heavy atom method and refined by a full-matrix least-squares technique. Occupancy factors of Br atoms were included in the calculations. Weighting scheme is  $w = [\sigma^2 + (0.015 \times |F_o|)^2]^{-1}$ . Final *R* and *R<sub>w</sub>* values are 0.035 and 0.034 for 1043 room temperature data ( $2\theta \leq 65^\circ$ ,  $|F_o| \geq 3\sigma(F_o)$ ), and 0.037 and 0.034 for 1261 low-temperature data ( $2\theta \leq 90^\circ$ ,  $|F_o| \geq 3\sigma(F_o)$ ), respectively.

(11) X-ray structure analysis has been made by using an orange-red prism with dimensions of  $0.36 \times 0.11 \times 0.08$  mm at room temperature. Crystal data are as follows: (2)  $\text{C}_{10}\text{H}_{24}\text{N}_4\text{NiBr}_2\text{ClO}_4$ , orthorhombic, *P*2<sub>1</sub>2<sub>1</sub>2<sub>1</sub>, *Z* = 4, *a* = 13.282 (2) Å, *b* = 19.451 (4) Å, *c* = 6.745 (1) Å, *V* = 1742.6 (5) Å<sup>3</sup>, *D<sub>x</sub>* = 1.976 g cm<sup>-3</sup>,  $\mu(\text{Mo K}\alpha)$  = 61.46 cm<sup>-1</sup>. Intensity data were measured by the same way as in ref 9. The structure was solved by a heavy atom method and refined by a block-diagonal least-squares method. Current *R* and *R<sub>w</sub>* values are 0.042 and 0.037, respectively, for 3663 independent reflections ( $2\theta < 65^\circ$ ,  $|F_o| \geq 3\sigma(F_o)$ ).

(12) Elemental analysis for **1**. Calcd for  $\text{C}_{12}\text{H}_{28}\text{N}_4\text{NiBr}_3$ : C, 27.36; H, 5.36; N, 10.64; Ni, 11.14; Br, 45.51. Found: C, 27.27; H, 5.40; N, 10.41; Br, 45.00.

(13) The density of **1** was determined by flotation with a mixture of  $\text{C}_2\text{H}_4\text{Br}_2$  and  $\text{CCl}_4$ .

(14) Larsen, K. P.; Toftlund, H. *Acta Chem. Scand., Sect. A* **1977**, *A31*, 182-186.

(15) Butler, L. G.; Zietlow, M. H.; Che, C.-M.; Schaefer, W. P.; Sridhar, S.; Grunthaler, P. J.; Swanson, B. I.; Clark, R. J. H.; Gray, H. B. *J. Am. Chem. Soc.* **1988**, *110*, 1155-1162.

(16) An X-ray structure analysis cannot give an unambiguous result with respect to the bridging Br position. This is due to the series-termination effect; atoms which are closer than  $\Delta r = 0.61\lambda/(2 \sin \theta_{\text{max}})$  are unresolved in a Fourier synthesis and appear as a single atom: James, R. W. *Acta Crystallogr.* **1948**, *1*, 132-134.

compound **2** (2.616 (1) Å). Secondly, the structure analysis of **1** does not indicate positional disorder of the bridging Br atom. The thermal ellipsoid of the bridging Br atom is very small ( $U_{\text{eq}}(-152^\circ\text{C}) = 0.0089 \text{ \AA}^2$ ). Finally, neither diffuse scattering nor satellite peak relating to a superstructure have been observed on the X-ray oscillation and Weissenberg photographs of **1**.

Semiconductive character of **1** has been revealed by optical and electrical conductivity measurements.<sup>17,18</sup> The single-crystal reflectivity measurement gave an optical energy gap of 1.28 eV.<sup>19</sup>

The magnetic susceptibility of aligned small crystals of **1** was also measured by a Faraday balance method in the temperature range 2-300 K.<sup>20</sup> The observed temperature independent isotropic magnetic susceptibility, which is less than  $10^{-7}$  emu g<sup>-1</sup>, does not correspond to a Pauli paramagnetism.<sup>21</sup> The magnetic behavior of **1** implies strong antiferromagnetic coupling between electronic spins (*S* = 1/2) localized on the Ni atoms of the bromo-bridged  $\text{Ni}^{\text{III}}\text{-X}\text{-Ni}^{\text{III}}$  linear chain. The two-dimensionality of the hydrogen bond network may play an important role in the magnetic structure. Further studies on the physical properties of **1** are now in progress.

**Supplementary Material Available:** Listings of fractional coordinates, isotropic and anisotropic thermal parameters, bond distances, bond angles, and hydrogen bond distances and ORTEP drawings of crystal and molecular structures (12 pages). Ordering information is given on any current masthead page.

(17) Measurements of the single-crystal electrical conductivity by four-probe technique, in which the electrical contacts were made with carbon paint, showed semiconducting behavior with a room temperature conductivity of  $2 \times 10^{-2} \Omega^{-1} \text{ cm}^{-1}$  and an activation energy of 0.11 eV along the *b* axis. The high conductivity and the small activation energy may be due to some impurities.

(18) The optical energy gap was obtained from the imaginary part of dielectric constant calculated from the reflectivity spectra by the Kramers-Kronig transformation.

(19) Luminescence or resonance Raman spectra have not yet been observed for **1**.

(20) Small crystals aligned on a quartz plate were used in the measurement.

(21) A small paramagnetic component which obeys the Curie law has been observed in the magnetic susceptibility measurement. The single-crystal EPR spectra, which were measured at 10 K for the aligned crystal of **1**, gave anisotropic *g* values of 2.178 and 2.029 for parallel and perpendicular components, respectively. The number of spins corresponds to 1 wt % of discrete  $\text{Ni}^{\text{III}}$  complex.

## The Sonochemistry of Zn Powder

Kenneth S. Suslick\* and Stephen J. Doktycz

School of Chemical Sciences  
University of Illinois at Urbana-Champaign  
505 South Mathews Avenue  
Urbana, Illinois 61801

Received August 22, 1988

High-intensity ultrasound can enhance both homogeneous and heterogeneous reactions.<sup>1-13</sup> It has found an important niche in

(1) (a) Suslick, K. S.; Doktycz, S. J. In *Advances in Sonochemistry*; Mason, T. J., Ed.; JAI Press: New York, 1989; Vol. 1, in press. (b) *Ultrasound: Its Chemical, Physical and Biological Effects*; Suslick, K. S., Ed.; VCH: New York, 1988. (c) Lindley, J.; Mason, T. J. *Chem. Soc. Rev.* **1987**, *16*, 275. (d) Suslick, K. S. *Adv. Organometallic Chem.* **1986**, *25*, 73. (e) Suslick, K. S. *Modern Synthetic Methods* **1986**, *4*, 1. (f) Boudjouk, P. J. *Chem. Ed.* **1986**, *63*, 427. (g) Margulis, M. A. *Ultrasonics* **1985**, *23*, 157. (h) Suslick, K. S. *Sci. Am.* **1989**, *260* (2), 80.

(2) (a) Boudjouk, P. In *High Energy Processes in Organometallic Chemistry*; Suslick, K. S., Ed.; ACS Symposium Series 333; American Chemical Society: Washington, DC, 1987; pp 209-222. (b) Boudjouk, P.; Han, B. H. *J. Catal.* **1983**, *79*, 489. (c) Han, B.-H.; Boudjouk, P. *Organomet.* **1983**, *2*, 769.

(3) (a) Boudjouk, P.; Han, B. H. *J. Org. Chem.* **1982**, *47*, 5030. (b) Han, B. H.; Boudjouk, P. *J. Org. Chem.* **1982**, *47*, 751. (c) Boudjouk, P.; Thompson, D. P.; Ohrbom, W. H.; Han, B. H. *Organomet.* **1986**, *5*, 1257.

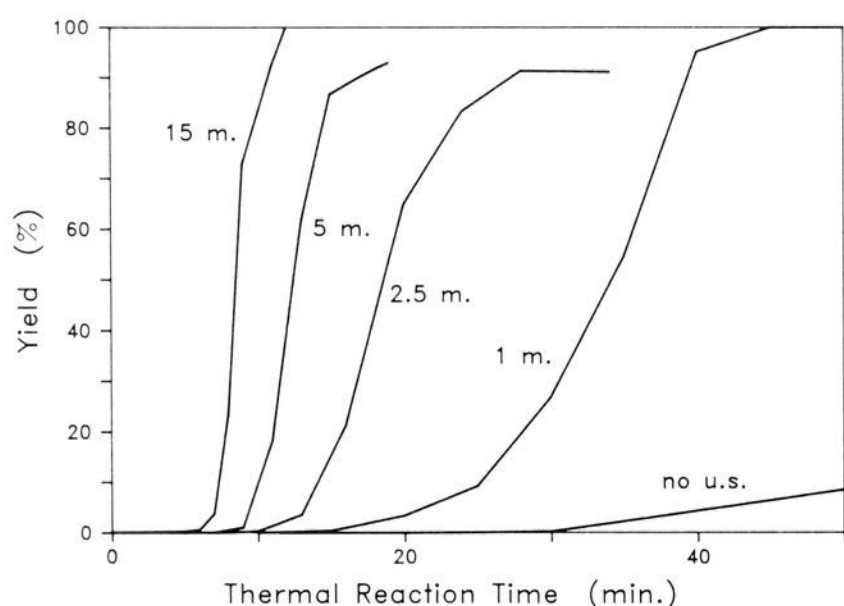


**Figure 1.** The effect of ultrasonic irradiation on the Reformatsky reaction. Zn powder (5  $\mu\text{m}$  mean diameter, Aldrich Chemicals) was irradiated in dioxane at 16  $^{\circ}\text{C}$  for increasing lengths of time, as indicated. Reactants were then added (1:1.2:3.0 molar ratio of benzaldehyde, ethyl bromoacetate, and Zn) and product monitored by GC-MS.

organic synthesis using reactive metals.<sup>3-9</sup> Most investigations of heterogeneous sonochemistry, however, have been strictly descriptive. Although a detailed understanding of homogeneous sonochemistry has been recently developed,<sup>12,13</sup> our knowledge about the effects of ultrasound on liquid–solid interfaces is much more limited.<sup>1,9,10a</sup> To better understand the origin of heterogeneous sonochemistry, we have examined the effects of ultrasonic irradiation on chemical reactivity, particle and surface morphology, and surface atomic composition of Zn powder. We believe that the observed changes are primarily due to interparticle collisions which result from the turbulent flow and shockwaves produced by the ultrasonic field.

Ultrasound in liquids creates acoustic cavitation, i.e., the formation, growth, and implosive collapse of bubbles.<sup>1</sup> When acoustic cavitation occurs near an extended liquid–solid interface, markedly asymmetric bubble collapse occurs, which generates a high speed jet of liquid directed at the surface.<sup>14</sup> The impingement of this jet and related shockwaves can create localized erosion,<sup>14,15</sup> cause

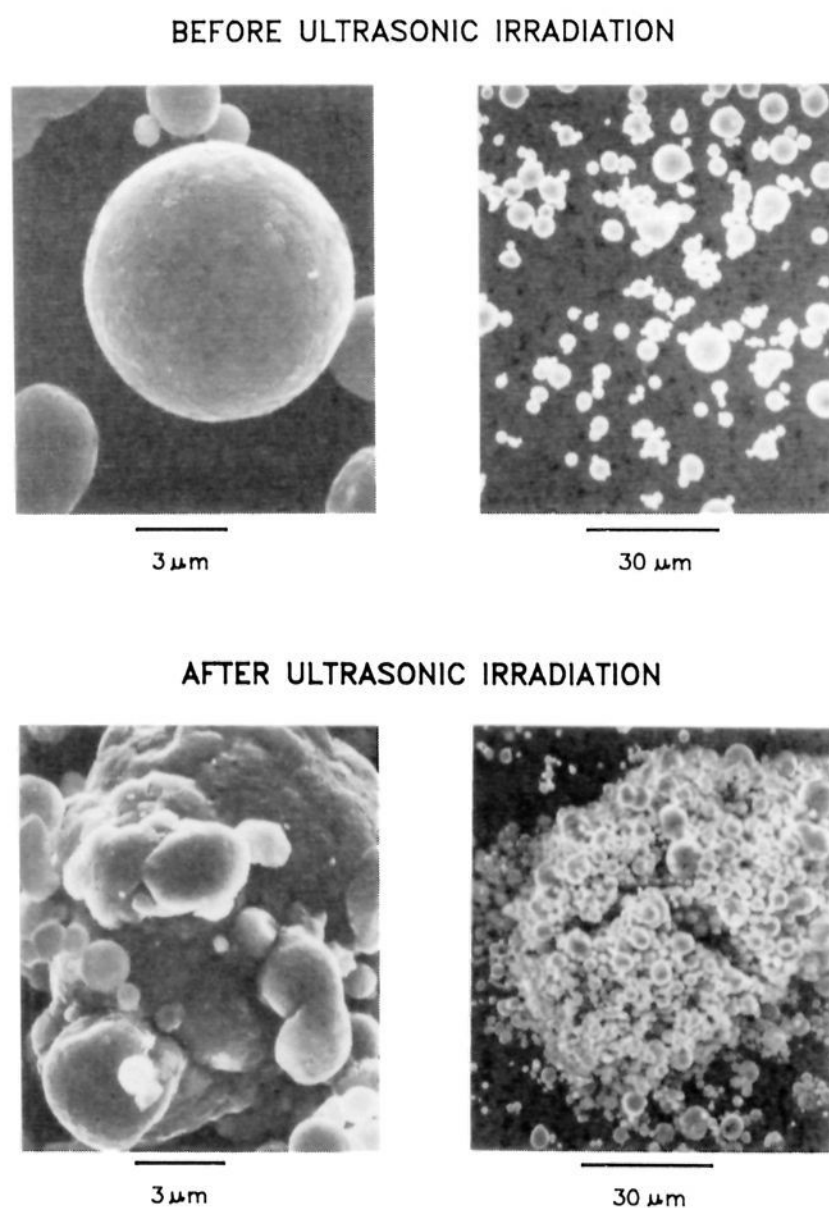


**Figure 2.** Scanning electron micrographs of Zn powder (5  $\mu\text{m}$  mean diameter) before and after ultrasonic irradiation, obtained on a Hitachi S-800 SEM.

particle fragmentation,<sup>16</sup> and improve mass transport.<sup>1b</sup> In the presence of fine powders, shockwaves and turbulent flow from cavitation can result in interparticle collisions of the solids. Such collisions can occur with enough force to cause changes in surface area, morphology, and composition of the powders.<sup>1a,9,10a</sup>

Previous studies have demonstrated the efficacy of ultrasound in various reactions involving Zn, including conjugate addition to  $\alpha$ -enones,<sup>4</sup> carboxylation of perfluoroalkyls,<sup>5</sup> cyclopropanation,<sup>6</sup> and the Reformatsky reaction.<sup>3</sup> For example, Boudjouk and Han<sup>3b</sup> found that low intensity ultrasound (from a cleaning bath) significantly increased Reformatsky reaction rates and yields (typically 30 min and >90% yield) and eliminated the need for specially activated Zn powders.<sup>17</sup> The use of iodine promoters, however, was reported to be important for optimal yields. No attempt, however, was made to discern the origin of the effects of ultrasound.

As part of our studies on the chemical effects of ultrasound, we have used as a mechanistic probe the Reformatsky reaction of benzaldehyde and ethyl bromoacetate with Zn. High intensity ultrasound from a direct immersion horn ( $\approx 50 \text{ W}/\text{cm}^2$ , described elsewhere<sup>18</sup>) has a considerably greater effect than an ultrasonic

(4) (a) Luche, J. L.; Petrier, C.; Lansard, J. L.; Greene, E. A. *J. Org. Chem.* **1983**, *48*, 3837. (b) Petrier, C.; Luche, J. L.; Dupuy, C. *Tetrahedron Lett.* **1984**, *25*, 3463. (c) Greene, A. E.; Lansard, J. P.; Luche, J. L.; Petrier, C. *J. Org. Chem.* **1984**, *49*, 931.

(5) (a) Kitazume, T.; Ishikawa, N. *Chem. Lett.* **1981**, 1679. (b) Kitazume, T.; Ishikawa, N. *Chem. Lett.* **1982**, 137. (c) Kitazume, T.; Ishikawa, N. *Chem. Lett.* **1984**, 1453.

(6) Repic, O.; Vogt, S. *Tetrahedron Lett.* **1982**, *23*, 2729.

(7) (a) Luche, J. L. *Ultrasonics* **1987**, *25*, 40. (b) Petrier, C.; Dupuy, C.; Luche, J. L. *Tetrahedron Lett.* **1986**, *27*, 3149. (c) Petrier, C.; Barbosa, J. C.; Dupuy, C.; Luche, J. L. *J. Org. Chem.* **1985**, *50*, 910, 5761. (d) Luche, J. L.; Damiano, J. C. *J. Am. Chem. Soc.* **1980**, *102*, 7926.

(8) (a) Bonnemant, H.; Bogdanovic, B.; Brinkman, R.; He, D. W.; Spliethoff, B. *Angew. Chem., Int. Ed. Engl.* **1983**, *22*, 728. (b) Lindley, J.; Mason, T. J.; Lorimer, J. P. *Ultrasonics* **1987**, *25*, 45.

(9) (a) Suslick, K. S.; Doktycz, S. J. *Chem. Mater.* **1989**, *1*(1), 6. (b) Suslick, K. S.; Casadonte, D. J.; Doktycz, S. J. *Solid State Ionics* **1989**, *32*, in press.

(10) (a) Suslick, K. S.; Casadonte, D. J. *J. Am. Chem. Soc.* **1987**, *109*, 3459. (b) Cioffi, E. A.; Prestegard, J. H. *Tetrahedron Lett.* **1986**, *27*, 415. (c) Moulton, K. J., Jr.; Koritala, S.; Frankel, E. N. *J. Am. Oil Chem. Soc.* **1983**, *60*, 1257. (d) Saracco, G.; Arzano, F. *Chim. Ind. (Milan)* **1968**, *50*, 314. (e) Slaczka, A. *Int. Chem. Eng.* **1969**, *9*, 63.

(11) (a) Ando, T.; Sumi, S.; Kawate, T.; Ichihara, J.; Hanafusa, T. *J. Chem. Soc., Chem. Commun.* **1984**, 439. (b) Chou, T.-S.; Tsao, C.-H.; Hung, S. C. *J. Org. Chem.* **1985**, *50*, 4329.

(12) (a) Suslick, K. S.; Goodale, J. W.; Wang, H. H.; Schubert, P. F. *J. Am. Chem. Soc.* **1983**, *105*, 5781. (b) Suslick, K. S.; Schubert, P. F. *J. Am. Chem. Soc.* **1983**, *105*, 6042. (c) Suslick, K. S. In *High Energy Processes in Organometallic Chemistry*; Suslick, K. S., Ed.; ACS Symposium Series 333; American Chemical Society: Washington, DC, 1987; p 191.

(13) (a) Suslick, K. S.; Flint, E. B. *Nature* **1987**, *330*, 553. (b) Suslick, K. S.; Cline, R. E., Jr.; Hammerton, D. A. *J. Am. Chem. Soc.* **1986**, *108*, 5641. (c) Suslick, K. S.; Hammerton, D. A. *I.E.E.E. Trans. Ultrason. Ferroelec., Freq. Cont.* **1986**, *33*, 143. (d) Suslick, K. S.; Gawienowski, J. W.; Schubert, P. F.; Wang, H. H. *J. Phys. Chem.* **1983**, *87*, 2299.

(14) (a) Benjamin, T. B. *Philos. Trans* **1966**, *A260*, 221. (b) Lauterborn, W.; Hentschel, W. *Ultrasonics* **1985**, *24*, 59. (c) Preece, C. M.; Hansson, I. L. *Adv. Mech. Phys. Surf.* **1981**, *1*, 199.

(15) de Souza-Baroza, J. C.; Petrier, C.; Luche, J. L. *J. Org. Chem.* **1988**, *53*, 1212.

(16) (a) Suslick, K. S.; Casadonte, D. J.; Green, M. L. H.; Thompson, M. E. *Ultrasonics* **1987**, *25*, 56. (b) Suslick, K. S.; Green, M. L. H.; Thompson, M. E.; Chatakonda, K. *J. Chem. Soc., Chem. Commun.* **1987**, 900.

(17) (a) Rieke, R. D.; Uhm, S. J. *Synthesis* **1975**, 452. (b) Rieke, R. D.; Burns, T. P.; Wehmeyer, R. M.; Kahn, B. E. In *High Energy Processes in Organometallic Chemistry*; Suslick, K. S., Ed.; ACS Symposium Series 333; American Chemical Society: Washington, DC, 1987; p 223.

(18) Suslick, K. S.; Flint, E. B. In *Experimental Organometallic Chemistry*; Wayda, A.; Darenbourg, M. Y., Eds.; ACS Symposium Series 357; American Chemical Society: Washington, DC, 1987; p 195.

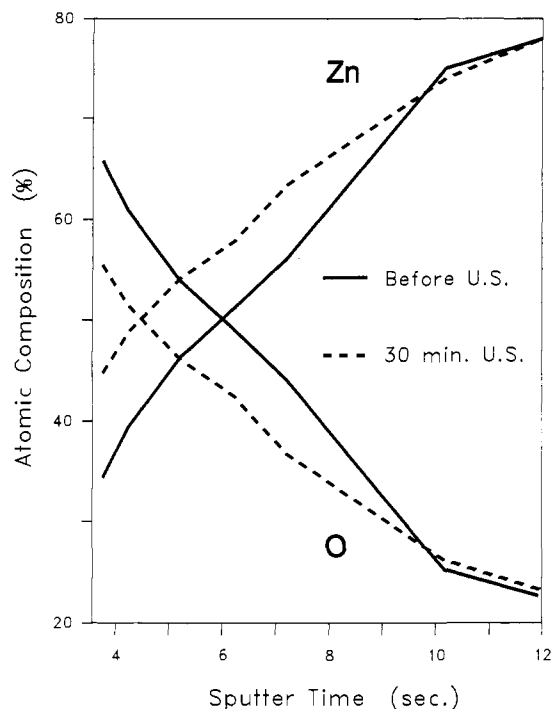
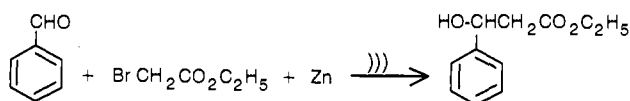


**Figure 3.** Atomic composition depth profiles of Zn pellets before and after ultrasonic irradiation, as determined by sputtered neutral mass spectrometry. These data are a composite of many particles in the pellet at varying depths into each particle and therefore quantitatively underestimate the decrease in the oxide coating after ultrasonic irradiation. SNMS was chosen for these analyses because the propensity of Zn metal to volatilize in an electron beam precludes the use of other surface characterization techniques capable of better spatial resolution.

cleaning bath ( $<10 \text{ W/cm}^2$ ). When the complete reaction mixture is irradiated,<sup>19</sup> yields are  $>95\%$  after 5 min at  $25^\circ\text{C}$ . In contrast to previous work, iodine promotion had no effect in yield or reaction time.



The effects of ultrasound are equally significant if the Zn powder is irradiated *before* the addition of substrate (Figure 1). The observed maximum rates (which occur at roughly 50% of completion) increase approximately 50-fold after ultrasonic irradiation for 15.0 min.<sup>19b</sup> In addition, the induction period observed is greatly reduced: in the absence of ultrasound, 1% product is formed only after more than 30 min; after 15 min irradiation, 1% product requires only 6 min.<sup>19c</sup>

This increase in activity is not due to increased surface area. Three-point B.E.T. determinations on irradiated Zn powders show only small increases in surface area (for 0-, 5-, 15-, and 30-min irradiation, 0.40, 0.46, 0.48, and  $0.60 \text{ m}^2/\text{g} \pm 5\%$ ), which cannot account for the large increase in reaction rates.

Scanning electron micrographs were taken of irradiated Zn samples (Figure 2). Dramatic changes in particle morphology and aggregation are observed. The Zn particles initially are extremely smooth and spherical, but upon sonication the surface is noticeably roughened. At the same time, particle agglomeration

(19) (a) Each reaction solution was diluted with benzene, shaken with ice water, and neutralized with excess concentrated  $\text{NH}_3(\text{aq})$  until redissolution of the zinc salts occurred. The organic layer was isolated and diluted to a known volume; internal standard was then added, and the solution was analyzed by GC-MS on an HP 5970. (b) The interpolated maximum rates are 4.5, 24.5, 48.6, 97.2, and  $220 \text{ mM/min}$  after prior irradiation for 0.0, 1.0, 2.5, 5.0, and 15.0 min, respectively. (c) The interpolated induction times for formation of 1% product are 31.5, 16.0, 10.5, 8.5, and 6.0 min after prior irradiation for 0.0, 1.0, 2.5, 5.0 and 15.0 min, respectively. Interpolated induction times for the formation of 5% product are 41.0, 21.5, 13.0, 9.5, and 7.0 min, for the same conditions.

occurs, forming  $\approx 50 \mu\text{m}$  aggregates within 30 min of irradiation.

Associated with these changes in surface morphology are changes in surface composition. Elemental depth profiles using sputtered neutral mass spectrometry<sup>20</sup> (SNMS) were obtained on Zn powders before and after ultrasonic irradiation (Figure 3). The appreciable oxide coating initially present on the Zn powder is significantly reduced after irradiation.

We believe that the observed changes in particle morphology, aggregation, and surface composition are due to high-velocity interparticle collisions. Ultrasonic irradiation of liquid-solid slurries creates shockwaves and turbulent flow which produces such collisions. If particles collide head-on, they can do so with enough energy to cause localized melting at the point of contact. This results in particle agglomeration and in the exposure of highly reactive Zn metal. If particles collide at a glancing angle, increased surface roughness and cracking of the oxide layer can result.<sup>1a,9</sup> The sonochemical activation of Zn powder comes from the loss of oxide passivation.

**Acknowledgment.** We appreciate the assistance of Dr. Irena Dulmer and Dr. Christopher Loxton at the Center for Microanalysis of Materials, UIUC, supported by the DOE under contract DE-AC-02-76ER-01198. Support of the National Science Foundation is greatly appreciated. K.S.S. gratefully acknowledges an N.I.H. Research Career Development Award and a Sloan Foundation Research Fellowship.

(20) (a) Oechsner, H. In *Thin Film and Depth Profiling Analysis*; Oechsner, H., Ed.; Springer: New York, 1983. (b) Reuter, W. In *SIMS V*; Benninghoven, A., Colton, R. J., Simons, S., Werner, H. W., Eds.; Springer: New York, 1986; pp 44, 94.

### Metalloselective Anti-Porphyrin Monoclonal Antibodies

Alan W. Schwabacher,\*<sup>1</sup> Michael I. Weinhouse,  
Maria-Teresa M. Auditor, and Richard A. Lerner

Department of Molecular Biology  
Research Institute of Scripps Clinic  
10666 North Torrey Pines Road  
La Jolla, California 92037  
Received October 12, 1988

Antibodies raised against transition-state analogues have recently been shown to catalyze acyl transfers and sigmatropic reactions.<sup>2</sup> This promising approach to enzyme-like catalysts can be extended in several ways. Different transition-state analogues will lead to antibodies catalyzing other reactions, and site-directed mutagenesis will undoubtedly allow improvement of catalytic efficiency and mechanistic understanding. Cofactors provide another approach.

Enzymes use cofactors to catalyze a wider variety of reactions than would be possible with protein alone.<sup>3</sup> Among the most versatile and interesting of these cofactors are the metalloporphyrins.<sup>4</sup> Synthetic metalloporphyrins can hydroxylate alkanes, mimicking the function of cytochrome P-450,<sup>5</sup> for example, but without the enzymatic specificity. We want to use antibody binding specificity to add substrate, regio-, and enantioselectivity to reactions catalyzed by metalloporphyrins.

Possibly an antibody raised against a porphyrin-substrate complex would have a binding site complementary to both and after binding to porphyrin would allow attack on only the correctly

(1) Address correspondence to this author at Department of Chemistry, Iowa State University, Ames, Iowa 50011.

(2) Janda, K.; Schloeder, D.; Lerner, R.; Benkovic, S. *Science* **1988**, *241*, 1187. Hilvert, D.; Nared, K. *J. Am. Chem. Soc.* **1988**, *110*, 5593. Schultz, P. G. *Science* **1988**, *240*, 426 and references therein.

(3) Walsh, C. *Enzymatic Reaction Mechanisms*; W. H. Freeman and Company: 1979.

(4) Dixon, M.; Webb, E. C. *Enzymes*, 3rd Ed.; Academic Press: 1979; Chapter IX.

(5) Groves, J. T.; Nemo, T. E. *J. Am. Chem. Soc.* **1983**, *105*, 6243.